

# Complete dynamic model of the Twin Rotor MIMO System (TRMS) with experimental validation

Azamat Tastemirov<sup>\*,1</sup>, Andrea Lecchini-Visintini<sup>\*,2</sup> and Rafael M. Morales<sup>\*,3</sup>

<sup>\*</sup>Dept. of Engineering, University of Leicester, University Rd., Leicester, UK, LE1 7RH, UK

<sup>1</sup>azamat.tastemirov@gmail.com, <sup>2</sup>alv1@le.ac.uk, <sup>3</sup>rmm23@le.ac.uk

## Abstract

In this paper we develop a complete dynamic model of the Twin Rotor MIMO System (TRMS) using the Euler-Lagrange method. Our model improves upon the model provided by the manufacturer in the user manual and upon previous models of the TRMS which can be found in the literature. The model is tuned and validated using experimental data.

## 1 INTRODUCTION

The Twin Rotor MIMO Systems (TRMS) is a beam rotating freely in the vertical plane (pitch) about the end of a pivoted beam, which in turn rotates in the horizontal plane (yaw) about a fixed point. The beam is damped by a perpendicular counterbalance beam rigidly fixed in its centre. The beam is driven by two mutually perpendicular propellers located at its ends and driven by DC motors. The larger propeller with vertical axis is called the main rotor, and the half of the beam to which it is attached is called the main beam. The second propeller, and its corresponding half of the beam, are called the tail rotor and tail beam respectively. The pitch angles of the propeller blades are fixed, thus the propulsive force is governed by the propeller speed of rotation. The TRMS laboratory setup used in this work is manufactured by Feedback Instruments and is shown in Fig. 1.

The TRMS modelling and control problems have attracted a great attention during the last decade due to the highly non-linear and cross-coupled dynamics of the system. The application of the Newtonian approach to such system requires taking into account a variety of fictitious forces, the parameters of which are not readily available, while the Euler-Lagrange approach provides a rigorous and natural way to obtain dynamical equations. The simplified Newtonian models provided by the manufacturer in [2] and [3] do not capture the system's dynamics precisely. An extensive attempt to overcome the limitations of these models was made in [8], where an updated version of the Newtonian model of [2] and a more accurate model, derived using the Euler-Lagrange method, were pre-



Figure 1: Twin rotor MIMO setup

sented. However the models obtained in [8] still have a number of drawbacks. In these models, the propellers reactive torques, which are the main source of cross-coupling between the pitch and yaw angles, are not considered properly. In the Newtonian model, the use of the law of conservation of angular momentum to relate the rotors and body dynamics (see eqs. (8) and (12) in [8]) is not justified. In the Euler-Lagrange derivations, the kinetic energy of the rotors is not in-

cluded in the Lagrangian, instead, terms containing the rotors acceleration are included, without justification, as external torques (see eqs. (39) and (41) in [8]). Finally, all the vector quantities, used to calculate the kinetic energy of each part of the TRMS in [8], are expressed in terms of global inertial frame, which leads to unnecessarily complicated calculations. Another application of the Euler-Lagrange approach to the equations of motion of TRMS was reported in [6] but, unfortunately, the authors did not disclose the details of the derivation and presented only the final equations, in their most general form, and without specifying the numerical values of the parameters. Here we adopt the modelling methodology presented in [7], where it was applied to a similar system called Toycopter. The main advantage of this methodology is that the vector quantities characterising the translating parts are expressed in the body-fixed frame of reference, which significantly simplifies calculation of the kinetic energy. The main structural difference between the Toycopter and the TRMS is the presence of the pivoted beam, of the counterbalance beam, and of a flat cable, in the latter, which result in more complex derivations and final dynamical equations.

## 2 TWIN ROTOR DYNAMICS

We will first obtain the equations describing the DC motors and then the equations of motion of the mechanical parts.

### 2.1 DC motors

The main and tail DC motors are assumed to be completely identical, therefore, all the equations in this section will be given in general form and can easily be applied to the considered motor by adding the subscript “m” or “t”. The voltage of the DC motor, denoted as  $v$ , is set in Simulink through the control signal  $u$ . The entire channel from the control signal to the motor voltage is assumed to have a constant gain, i.e.  $v = k_u u$ . The DC motor itself is described by a simple first-order differential equation

$$(1) \quad L_m \frac{di}{dt} = v - k_v \omega - Ri$$

where:

- $i$ : is the motor current,
- $L_m$ : is the motor inductance,
- $R$ : is the motor resistance,
- $k_v$ : is the motor back EMF constant,
- $\omega$ : is the motor angular velocity.

By comparing the numerical values of the electrical and mechanical time constants of, for example,

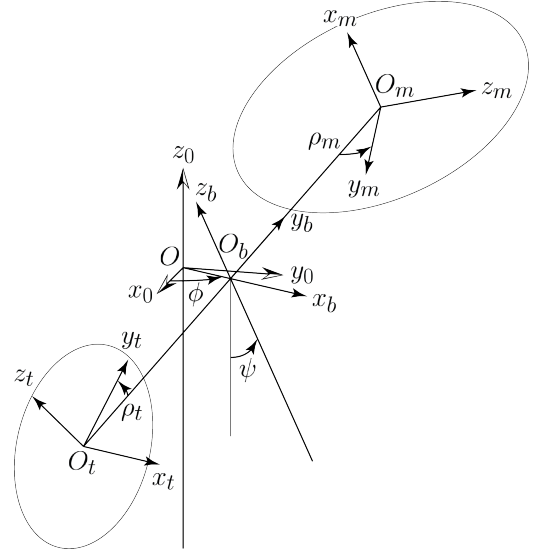


Figure 2: TRMS notation

the main rotor

$$(2) \quad c_e = \frac{L_m}{R} = 1.075 \times 10^{-4} \text{ s} \quad c_m = \frac{I_1 R}{k_t k_v} = 3.38 \text{ s}$$

(where  $I_1$  is the rotor’s moment of inertia, which value will be calculated below), we note that the dynamics of the motor’s current can be neglected, resulting in the following algebraic equation for the DC motor circuit:

$$(3) \quad v - k_v \omega - Ri = 0.$$

### 2.2 Rigid Body

The Euler-Lagrange method involves the following steps [1]:

1. Define a set of generalised coordinates  $\mathbf{q} = \{q_1, \dots, q_n\}$
2. Find the kinetic energy  $T(\mathbf{q}, \dot{\mathbf{q}}, t)$ , the potential energy  $U(\mathbf{q}, t)$ , and the Lagrangian  $L(\mathbf{q}, \dot{\mathbf{q}}, t) = T - U$
3. For each coordinate find the generalised force  $F_{q_i}$
4. For each coordinate compute the Euler-Lagrange equation

$$(4) \quad \frac{d}{dt} \left( \frac{\partial L}{\partial \dot{q}_i} \right) - \frac{\partial L}{\partial q_i} = F_{q_i}.$$

The set of generalised coordinates is selected as  $\mathbf{q} = \{\psi, \phi, \rho_m, \rho_t\}$ , where  $\psi$  denote the pitch angle,  $\phi$  the yaw angle,  $\rho_m$  and  $\rho_t$  the angles of the main and tail rotors as shown in Fig. 2. The steps used to derive the Lagrangian are very similar to those used in [7] to model the Toycopter, with some differences which will be pointed out at the end of the section.

#### 2.2.1 Kinetic energy

Consider a rigid body, performing an arbitrary motion in three dimensional space. Let  $A$  denote an arbitrary

point fixed in the body,  $M$  denote the mass of the body and  $\mathbf{I}_A$  the inertia matrix with respect to the point  $A$ . Furthermore, let  $\mathbf{v}_A$  denote the instantaneous linear velocity vector of  $A$ ,  $\Omega$  the instantaneous angular velocity vector and  $\mathbf{r}_{AG}$  the vector between the centre of mass  $G$  and  $A$ . The kinetic energy of the rigid body can be obtained using the following general formula [7],[9, eq. (5.2)]:

$$(5) \quad T = \frac{1}{2} M \mathbf{v}_A^T \mathbf{v}_A + M \mathbf{v}_A^T (\Omega \times \mathbf{r}_{AG}) + \frac{1}{2} \Omega^T \mathbf{I}_A \Omega.$$

In order to calculate the total kinetic energy the TRMS will be considered consisting of four separate rigid bodies, namely: a) main rotor; b) tail rotor; c) body, comprising the main beam, tail beam, rotors shields and counterbalance beam with weight; and d) pivoted beam. Each rotor is formed by the corresponding propeller and DC motor rotor. In order to simplify the calculation of the kinetic energy, all vector quantities associated with each body are expressed in its body-fixed frame, i.e. reference frame attached to the body.

Let the body-fixed frame  $(x_m, y_m, z_m)$  of the main rotor be attached to its centre of mass  $O_m$  so that its  $x_m$ -axis coincides with the axis of rotation of the propeller and is directed upwards, and  $y_m$ -axis coincides with the propeller blade (Fig. 2). The main rotor angular velocity is determined as the vector sum of three angular velocities of rotation along  $\rho_m$ ,  $\psi$  and  $\phi$  angles as shown in Fig. 3:

$$(6) \quad \Omega_m = \begin{bmatrix} \dot{\rho}_m + \dot{\phi} \cos \psi \\ \dot{\psi} \sin \rho_m - \dot{\phi} \cos \rho_m \sin \psi \\ \dot{\psi} \cos \rho_m + \dot{\phi} \sin \rho_m \sin \psi \end{bmatrix}.$$

Let  $l_m$  denote the distance between the points  $O_b$  and  $O_m$  (which is also the length of the main beam) and  $d_m$  the distance between the points  $O$  and  $O_m$ . Translation of the point  $O_m$  is due to the rotation of the main beam along the  $\psi$  and  $\phi$  angles, therefore, the instantaneous linear velocity vector of the point  $O_m$  with respect to the body-fixed frame is (Fig. 4):

$$(7) \quad \mathbf{v}_m = \begin{bmatrix} l_m \dot{\psi} \\ -d_m \dot{\phi} \cos \psi \sin(\rho_m + \theta) \\ -d_m \dot{\phi} \cos \psi \cos(\rho_m + \theta) \end{bmatrix}$$

where  $\theta$  is a fixed angle determined as  $\arccos \frac{l_m}{d_m}$ . Under assumption of high rotational speed the tensor of inertia of the main rotor is diagonal and its components corresponding to the  $y_m$  and  $z_m$  axes can be taken equal:

$$(8) \quad \mathbf{I}_m = \begin{bmatrix} I_{m1} & 0 & 0 \\ 0 & I_{m23} & 0 \\ 0 & 0 & I_{m23} \end{bmatrix}.$$

Due to the choice of the body-fixed frame, the position vector (corresponding to  $\mathbf{r}_{AG}$  in (5)) vanishes.

Let  $h$  denote the distance between the points  $O_b$  and  $O$ . Applying the same approach to the tail rotor we obtain:

$$(9) \quad \Omega_t = [\dot{\psi} + \dot{\rho}_t \quad \dot{\phi} \sin(\psi + \rho_t) \quad \dot{\phi} \cos(\psi + \rho_t)]^T$$

$$(10) \quad \mathbf{v}_t = \begin{bmatrix} l_t \dot{\phi} \cos \psi \\ -l_t \dot{\psi} \sin \rho_t + h \dot{\phi} \cos \psi \cos \rho_t \\ -l_t \dot{\psi} \cos \rho_t - h \dot{\phi} \cos \psi \sin \rho_t \end{bmatrix}$$

$$(11) \quad \mathbf{I}_t = \begin{bmatrix} I_{t1} & 0 & 0 \\ 0 & I_{t23} & 0 \\ 0 & 0 & I_{t23} \end{bmatrix}.$$

Let the body-fixed frame  $(x_b, y_b, z_b)$  of the TRMS body be attached to point  $O_b$  as shown in Fig. 2. The angular velocity vector of the TRMS body with respect to the body-fixed frame is (Fig. 5a)

$$(12) \quad \Omega_b = [\dot{\psi} \quad \dot{\phi} \sin \psi \quad \dot{\phi} \cos \psi]^T,$$

and the linear velocity vector of the point  $O_b$  due to rotation of the TRMS body along  $\phi$  angle is (Fig. 5b)

$$(13) \quad \mathbf{v}_b = [0 \quad h \dot{\phi} \cos \psi \quad -h \dot{\phi} \sin \psi]^T.$$

Let  $G_b$  denote the centre of mass of the TRMS body. Due to symmetry  $G_b$  lies somewhere in the plane formed by the main and counterbalance beams. The

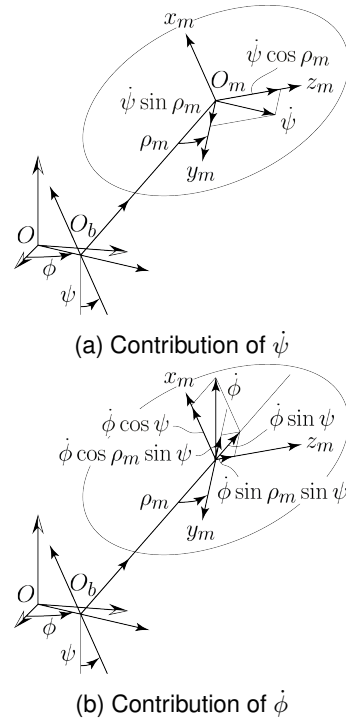


Figure 3: Calculation of the main rotor angular velocity ( $\Omega_m$ )

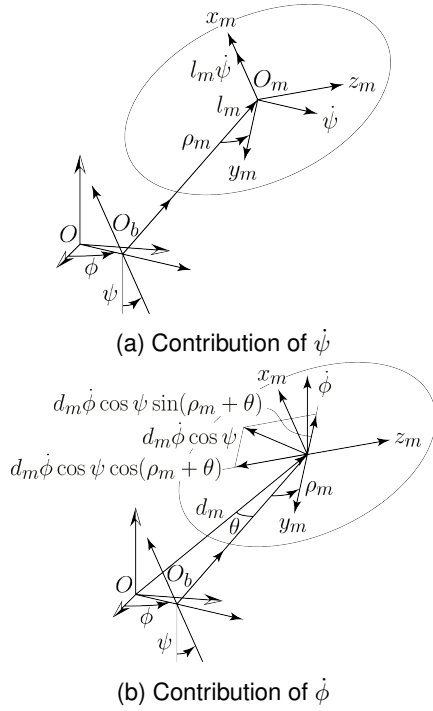


Figure 4: Calculation of the main rotor linear velocity ( $\mathbf{v}_m$ )

corresponding position vector, to be used in equation (5), is:

$$(14) \quad \mathbf{r}_{O_b G_b} = [0 \quad y_{Gb} \quad z_{Gb}]^T.$$

It can be easily demonstrated that the tensor of inertia of the TRMS body is diagonal of form:

$$(15) \quad \mathbf{I}_b = \begin{bmatrix} I_{b11} & 0 & 0 \\ 0 & I_{b22} & 0 \\ 0 & 0 & I_{b33} \end{bmatrix}.$$

Let  $M_m$ ,  $M_t$  and  $M_b$  denote the masses of the main rotor, of the tail rotor and of the TRMS body respectively. Expanding eq. (5) for each of the rigid bodies using the equations obtained above yields the follow-

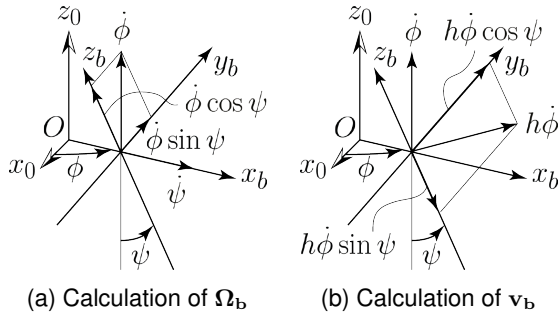


Figure 5: Calculation of the TRMS body angular velocity ( $\Omega_b$ ) and linear velocity ( $\mathbf{v}_m$ )

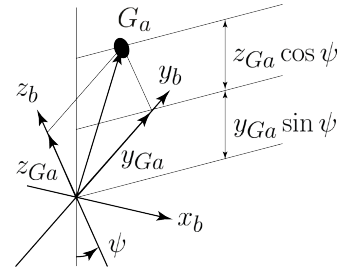


Figure 6: Vertical position of the centre of mass

ing equations for kinetic energy:

$$(16) \quad T_m = \frac{1}{2} I_{m23} \dot{\phi}^2 + \frac{1}{2} (I_{m23} + M_m l_m^2) \dot{\psi}^2 + \frac{1}{2} (I_{m1} - I_{m23} + M_m d_m^2) \dot{\phi}^2 \cos^2 \psi + \frac{1}{2} I_{m1} \dot{\rho}_m^2 + I_{m1} \dot{\phi} \dot{\rho}_m \cos \psi$$

$$(17) \quad T_t = \frac{1}{2} M_t d_t^2 \dot{\phi}^2 \cos^2 \psi + \frac{1}{2} (I_{t1} + M_t l_t^2) \dot{\psi}^2 + \frac{1}{2} I_{t23} \dot{\phi}^2 + I_{t1} \dot{\psi} \dot{\rho}_t + \frac{1}{2} I_{t1} \dot{\rho}_t^2$$

$$(18) \quad T_b = \frac{1}{2} I_{b11} \dot{\psi}^2 + \frac{1}{2} I_{b22} \dot{\phi}^2 \sin^2 \psi + \frac{1}{2} I_{b33} \dot{\phi}^2 \cos^2 \psi + \frac{1}{2} M_b \dot{\phi}^2 h^2 - M_b \dot{\phi} h (z_{Gb} \dot{\psi} \cos \psi + y_{Gb} \dot{\psi} \sin \psi).$$

The kinetic energy of the pivoted beam is simply:

$$(19) \quad T_p = \frac{1}{2} I_p \dot{\phi}^2.$$

## 2.2.2 Potential energy

In order to obtain the total potential energy we consider the aggregate body of mass  $M_a$  consisting of those parts which have a variable potential energy: the main rotor, tail rotor and body. Let  $G_a$  denote the centre of mass of the aggregate body. Due to symmetry, the position of  $G_a$  with respect to the body-fixed frame can be defined by two coordinates  $y_{G_a}$  and  $z_{G_a}$ . Expressing the vertical position of  $G_a$  relatively to the stationary point  $O$  in terms of  $y_{G_a}$  and  $z_{G_a}$  (Fig. 6) the potential energy takes the form:

$$(20) \quad V_a = M_a g (z_{G_a} \cos \psi + y_{G_a} \sin \psi).$$

## 2.2.3 Lagrangian

Expanding the Lagrangian  $L = T_m + T_t + T_b + T_p - V_a$  and grouping the constants in the resulting expression yields

$$(21a) \quad L = \frac{1}{2} I_\phi \dot{\phi}^2 + \frac{1}{2} I_c \dot{\phi}^2 \cos^2 \psi + \frac{1}{2} I_\psi \dot{\psi}^2$$

$$+ \frac{1}{2}I_{m1}\dot{\rho}_m^2 + \frac{1}{2}I_{t1}\dot{\rho}_t^2 - G_c \cos \psi - G_s \sin \psi \\ + I_{t1}\dot{\psi}\dot{\rho}_t + I_{m1}\dot{\phi}\dot{\rho}_m \cos \psi - H_c\dot{\phi}\dot{\psi} \cos \psi - H_s\dot{\phi}\dot{\psi} \sin \psi$$

where:

$$(21b) \quad G_c = M_a g z_{G_a}$$

$$(21c) \quad G_s = M_a g y_{G_a}$$

$$(21d) \quad H_c = M_b h z_{G_b}$$

$$(21e) \quad H_s = M_b h y_{G_b}$$

$$(21f) \quad I_\phi = I_{m23} + I_p + I_{t23} + I_{b22} + M_b h^2$$

$$(21g) \quad I_c = I_{b33} + I_{m1} - I_{m23} - I_{b22} + M_m d_m^2 +$$

$$(21h) \quad + M_t d_t^2$$

$$(21i) \quad I_\psi = I_{b11} + I_{m23} + I_{t1} + M_m l_m^2 + M_t l_t^2.$$

Let us recall that in the equations above  $h$  denotes the distance between the points  $O_b$  and  $O$ ,  $d_m$  denotes the distance between the points  $O$  and  $O_m$ , and  $d_t$  denotes the distance between the points  $O$  and  $O_t$ , and that  $d_m^2 = l_m^2 + h^2$  and  $d_t^2 = l_t^2 + h^2$ .

## 2.2.4 Generalized forces

The following forces are external to the TRMS: 1. the aerodynamic forces created by the propellers; 2. the electromechanical forces generated by DC motors; 3. the viscous forces due to friction in ball bearings; and 4. the elastic force created by the cable.

According to blade element theory [4], each rotating propeller generates the propulsive force (or thrust)  $T$  and the load torque  $Q$  which are both proportional to the square of the angular speed. The load torque  $Q$ , generated by air resistance on the blades of the propeller, is exerted on the corresponding DC motor's rotor, but has also the effect of rotating the TRMS body in the opposite direction to the spinning blades. Thus, the main propeller creates three different vector quantities, namely: the thrust torque of magnitude  $C_{Tm}\dot{\rho}_m |\dot{\rho}_m| l_m$ , acting along the  $\psi$  angle, the torque of magnitude  $-C_{Rm}\dot{\rho}_m |\dot{\rho}_m| \cos \psi$ , acting along the  $\phi$  angle, and the torque of magnitude  $C_{Qm}\dot{\rho}_m |\dot{\rho}_m|$  acting along the  $\rho_m$  angle. Similarly, the tail propeller creates the following torques:  $C_{Tr}\dot{\rho}_r |\dot{\rho}_r| l_t \cos \psi$  on  $\phi$  angle,  $-C_{Rt}\dot{\rho}_t |\dot{\rho}_t|$  on  $\psi$  angle and  $C_{Qt}\dot{\rho}_t |\dot{\rho}_t|$  on  $\rho_t$  angle.

The electromechanical torque generated by the DC motor is equal to  $k_t i$ , where  $k_t$  and  $i$  stand for motor torque constant and current respectively.

Friction is a complex phenomenon which encompasses a variety of effects. However, a simplified friction model, which takes into account only two major components, namely viscous and Coulomb friction, is usually utilised in the control of mechanical systems [5]. Assuming high rotational speed of the rotors, the Coulomb friction term for the corresponding coordinates can be neglected. Thus, the magnitudes of friction torques for each coordinate are

given by  $-(f_{v\psi}\dot{\psi} + f_{c\psi} \operatorname{sgn} \dot{\psi})$ ,  $-(f_{v\phi}\dot{\phi} + f_{c\phi} \operatorname{sgn} \dot{\phi})$ ,  $-f_{vm}\dot{\rho}_m$ ,  $-f_{vt}\dot{\rho}_t$ .

The flat cable, connecting the electrical equipment located on the moving parts of TRMS with the electronic board at the base of the setup possesses a certain stiffness and acts as a spring along the yaw angle. The magnitude of the torque exerted by the cable on yaw angle is taken as  $-C_c(\phi - \phi_0)$ .

Summing up all the forces mentioned above for each of generalised coordinates yields:

$$(22) \quad F_\psi = C_{Tm}\dot{\rho}_m |\dot{\rho}_m| l_m - C_{Rt}\dot{\rho}_t |\dot{\rho}_t| \\ - f_{v\psi}\dot{\psi} - f_{c\psi} \operatorname{sgn} \dot{\psi}$$

$$(23) \quad F_\phi = C_{Tr}\dot{\rho}_r |\dot{\rho}_r| l_t \cos \psi - C_{Rm}\dot{\rho}_m |\dot{\rho}_m| \cos \psi \\ - C_\phi\dot{\phi} - C_{\phi_0} \operatorname{sgn} \dot{\phi} - C_c(\phi - \phi_0)$$

$$(24) \quad F_{\rho_m} = k_{tm}i_m - f_{vm}\dot{\rho}_m - C_{Qm}\dot{\rho}_m |\dot{\rho}_m|$$

$$(25) \quad F_{\rho_t} = k_{tt}i_t - f_{vt}\dot{\rho}_t - C_{Qt}\dot{\rho}_t |\dot{\rho}_t|$$

## 2.2.5 Equations of motion

Finally, by computing eq. (4) in terms of each of generalised coordinates, we obtain the following equations of motion

$$(26) \quad I_\psi\ddot{\psi} = -I_{t1}\dot{\omega}_t + H_c\ddot{\phi} \cos \psi + H_s\ddot{\phi} \sin \psi \\ + G_c \sin \psi - G_s \cos \psi - \frac{1}{2}I_c\dot{\phi}^2 \sin(2\psi) \\ - I_{m1}\dot{\phi}\omega_m \sin \psi + C_{Tm}\omega_m |\omega_m| l_m - C_{Rt}\omega_t |\omega_t| \\ - f_{v\psi}\dot{\psi} - f_{c\psi} \operatorname{sgn} \dot{\psi}$$

$$(27) \quad (I_\phi + I_c \cos^2 \psi) \ddot{\phi} = -I_{m1}\dot{\omega}_m \cos \psi + H_c\ddot{\psi} \cos \psi \\ + H_s\ddot{\psi} \sin \psi + H_s\dot{\psi}^2 \cos \psi - H_c\dot{\psi}^2 \sin \psi + I_c \sin(2\psi) \dot{\phi}\dot{\psi} \\ + I_{m1}\omega_m \dot{\psi} \sin \psi + C_{Tr}\omega_t |\omega_t| l_t \cos \psi \\ - C_{Rm}\omega_m |\omega_m| \cos \psi - f_{v\phi}\dot{\phi} - f_{c\phi} \operatorname{sgn} \dot{\phi} - C_c(\phi - \phi_0)$$

$$(28) \quad I_{m1}\dot{\omega}_m = -I_{m1}\ddot{\phi} \cos \psi + k_{tm}i_m - f_{vm}\omega_m \\ - C_{Qm}\omega_m |\omega_m| + I_{m1}\dot{\phi}\dot{\psi} \sin \psi$$

$$(29) \quad I_{t1}\dot{\omega}_t = -I_{t1}\ddot{\psi} + k_{tt}i_t - f_{vt}\omega_t - C_{Qt}\omega_t |\omega_t|.$$

In the rotors' equations, i.e. (28) and (29), the terms involving the angular velocities and accelerations along  $\psi$  and  $\phi$  angles can be omitted assuming that their magnitudes are negligibly smaller than the rotors' accelerations. Thus, the simplified rotors' equations are:

$$(30) \quad I_{m1}\dot{\omega}_m = k_{tm}i_m - f_{vm}\omega_m - C_{Qm}\omega_m |\omega_m|$$

$$(31) \quad I_{t1}\dot{\omega}_t = k_{tt}\dot{i}_t - f_{vt}\omega_t - C_{Qt}\omega_t |\omega_t|.$$

It can be shown that for the particular case  $h = 0$  one recovers the equations of [7], with the additional term for the flat cable.

### 3 PARAMETERS

The next major step in the construction of the system's model is the estimation of the numerical values of its parameters. The initial parameters of the TRMS are provided in the User's Manual [3] and given in Table 1.

Table 1: TRMS parameters

parameter	value	unit
$l_t$	0.282	m
$l_m$	0.246	m
$l_b$	0.290	m
$l_{cb}$	0.276	m
$r_{ms}$	0.155	m
$r_{ts}$	0.100	m
$r_{mr}$	0.145	m
$r_{tr}$	0.090	m
$h$	0.06	m
$M_t$	0.221	kg
$M_m$	0.236	kg
$m_{cb}$	0.068	kg
$m_t$	0.015	kg
$m_m$	0.014	kg
$m_b$	0.022	kg
$m_{ts}$	0.119	kg
$m_{ms}$	0.219	kg
$m_h$	0.01	kg
$R_m, R_t$	8	$\Omega$
$L_{mm}, L_{mt}$	0.86	mH
$k_{vm}, k_{vt}$	0.0202	$\text{N m A}^{-1}$
$k_{tm}, k_{tt}$	0.0202	$\text{V rad}^{-1} \text{s}$
$k_{um}$	8.5	No units
$k_{ut}$	6.5	No units

#### 3.1 Propeller forces

The propellers thrust and reactive torque coefficients were measured experimentally using the methodology described in [2]. The experimental setup configuration for measuring the main propeller thrust is shown in Fig. 7 as an example. Electronic scales with a weight are placed under the beam and are attached to the main rotor as shown in Fig. 7. If necessary, a counterweight is added so that the measurements are taken when the system remains in horizontal equilibrium. In addition, the yaw angle must be fixed to avoid the effect of the reactive torque. The thrust of the

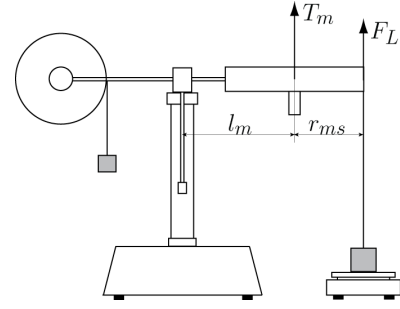


Figure 7: Measuring propellers thrusts for positive angular velocities

main propeller is obtained from the measured lifting force from the following relation:  $T_m = F_L \frac{(l_m + r_{ms})}{l_m}$ . The corresponding coefficient can be obtained using a least squares fitting of the experimental curve with a function of the form  $C\omega |\omega|$ , separately for positive and negative values of the rotor's speed (Fig. 8). The other coefficients are obtained in a similar way. Note, that in order to measure the tail rotor thrust and main rotor reactive torque the beam should be turned by 90 degrees. The measured values of the coefficients are given in Table 2, superscripts + and - denote the values corresponding to the positive and negative rotor speeds respectively.

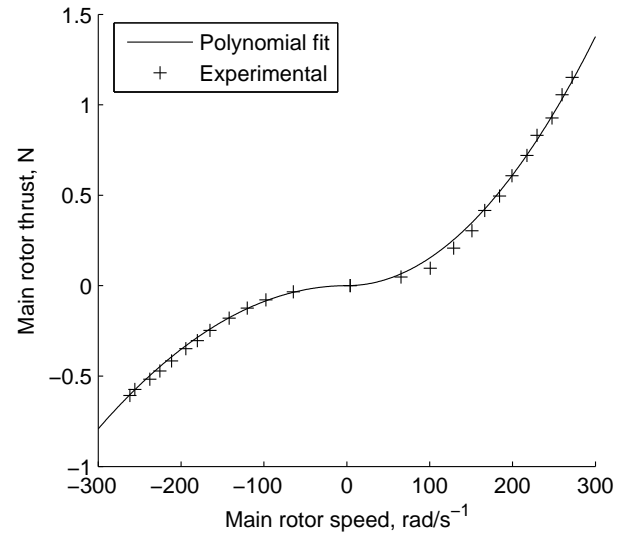


Figure 8: Main propeller static characteristic

#### 3.2 Friction coefficients

The measurements of the friction forces requires high-precision equipment and therefore they will not be considered in this work. The coefficients provided

by the User's manual on the TRMS [3] and by [8] are used instead.

### 3.3 Cable spring constant

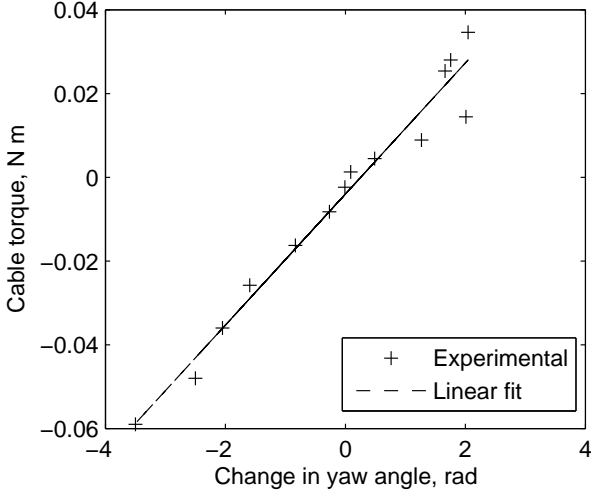


Figure 9: Cable characteristic

The stiffness coefficient of the cable is estimated experimentally using the procedure described below. First, the beam is locked in the horizontal position. Then, various values of the tail motor voltage are set in Simulink, and, after a constant yaw angle is attained, the tail rotor speed and change in yaw angle are recorded. The corresponding tail rotor thrust is calculated using its static characteristic. Taking all of the velocities except for the tail rotor angular velocity in eq. (27) equal to zero, we have a static equation governing the motion of the system during this experiment:

$$(32) \quad C_{T_t} \omega_t |\omega_t| l_t = C_c (\phi - \phi_0)$$

i.e. the torque created by the cable at a stationary yaw angle is equal to the one generated by the tail rotor. The resulting experimental plot is shown in Fig. 9. The estimated value of the cable spring constant obtained by linear least squares fitting is  $C_c = 0.016 \text{ N m rad}^{-1}$ . The steady yaw angle is taken as  $\phi_0 = -0.4602 \text{ rad}$ .

### 3.4 Parameters calculation

All the parameters considered in this section will be derived assuming that the system consists of simple geometric objects [2]. The main, tail and counterbalance beams are considered as thin rods, the main and tail shields as thin cylindrical shells with open ends, and the counterbalance weight as a point mass. The inertia matrix of the main rotor is diagonal due to its symmetry with respect to the body-fixed frame.

Furthermore, the main rotor is assumed to be: a thin rod of length  $2r_{mr}$  and mass  $M_m$  regarding to the axis of rotation, and, assuming high rotational speed, a thin disk of same mass and diameter regarding to the axes perpendicular to the axis of rotation [7]:

$$(33) \quad I_{m1} = \frac{1}{12} M_m r_{mr}^2, \quad I_{m23} = \frac{1}{4} M_m r_{mr}^2.$$

Similarly, for the tail rotor we have:

$$(34) \quad I_{t1} = \frac{1}{12} M_t r_{tr}^2, \quad I_{t23} = \frac{1}{4} M_t r_{tr}^2.$$

Clearly, this estimate of the moments of inertia is rough, and it will be adjusted further using a parameter optimisation procedure.

According to the superposition principle the inertia tensor of the TRMS body about the body-fixed reference frame is equal to the sum of inertia tensors of all constituent parts about the same frame. Thus, the TRMS body inertia tensor is given by

$$(35) \quad I_{b11} = \frac{1}{3} m_b l_b^2 + m_{cb} l_{cb}^2 + \frac{1}{3} m_m l_m^2 + m_{ms} l_m^2 + \frac{1}{3} m_t l_t^2 + m_{ts} l_t^2 + \frac{1}{2} m_{ms} r_{ms}^2 + m_{ts} r_{ts}^2$$

$$(36) \quad I_{b22} = \frac{1}{3} m_b l_b^2 + m_{cb} l_{cb}^2 + \frac{1}{2} m_{ms} r_{ms}^2 + \frac{1}{2} m_{ts} r_{ts}^2$$

$$(37) \quad I_{b33} = \frac{1}{3} m_m l_m^2 + m_{ms} l_m^2 + \frac{1}{3} m_t l_t^2 + m_{ts} l_t^2 + m_{ms} r_{ms}^2 + \frac{1}{2} m_{ts} r_{ts}^2.$$

The pivoted beam is assumed to be a thin rod of length  $h$  and mass  $m_h$ , thus the moment of inertia about the vertical axis through its end is given by

$$(38) \quad I_p = \frac{1}{3} m_h h^2.$$

The total mass of the TRMS body is given by

$$(39) \quad M_b = m_m + m_t + m_b + m_{ms} + m_{ts} + m_{cb},$$

and that of the aggregate body by:

$$(40) \quad M_a = M_b + M_m + M_t.$$

The coordinates of the centre of mass of the TRMS body are determined as

$$(41) \quad y_{Gb} = \frac{\frac{1}{2} l_m m_m + l_m m_{ms} - \frac{1}{2} l_t m_t - l_t m_{ts}}{M_b}$$

$$(42) \quad z_{Gb} = \frac{-\frac{1}{2} l_b m_b - l_{cb} m_{cb}}{M_b}.$$

Similarly, for the aggregate body we have:

$$(43) \quad y_{Ga} = \frac{\frac{1}{2}l_m m_m + l_m M_m + l_m m_{ms} - \frac{1}{2}l_t m_t - l_t M_t - l_t m_{ts}}{M_a}$$

$$(44) \quad z_{Ga} = \frac{-\frac{1}{2}l_b m_b - l_{cb} m_{cb}}{M_a}.$$

Expanding eqs. (21b)–(21g) and (21i) using the results of this section yields the final equations for the model parameters. The numerical values of the model parameters are given in Table 2.

### 3.5 Model tuning

The steady state pitch angle predicted by the model differs slightly from one displayed by the real plant  $\psi_0 = -0.5093$  rad. Clearly, the steady state pitch angle is determined solely by the coordinates of the centre of mass of the aggregate body estimated in eqs. (43) and (44). In fact, the centre of mass of the main rotor lies below  $y$ -axis, while in eq. (44) we assumed it lying on the  $y$ -axis, so the value of  $z_{Ga}$  should be tuned. Taking all the velocities in eq. (26) equal to zero, we have the following static equation revealing the steady state pitch angle

$$(45) \quad G_c \sin \psi - G_s \cos \psi = 0.$$

Combining eqs. (21b), (21c) and (45) yields:  $z_{Ga} = y_{Ga} \cot \psi_0 = -0.0307$  m. The updated value of depending parameter  $G_c$  is  $-0.2750$  N m.

Some of the model's parameters were optimised using a parameter estimation technique. The objective of the parameter estimation procedure is to find optimal values of the parameters under consideration according to some cost function, which is typically the least squares error between the experimental and model responses. In this work the Simulink Design Optimization toolbox was utilised. The optimisation of the parameters was carried out separately for the following four subsystems: the main rotor, tail rotor, pitch angle and the yaw angle. In each case considered, the subsystem was treated in an isolated and simplified mode of operation to avoid the effects of cross-couplings and of parameters not of interest. For example, the pitch angle subsystem was treated in 1DOF free response mode, i.e. with stopped rotors and fixed yaw angle. As a result, the following parameters were optimised:

- Main rotor: the moment of inertia  $I_{m1}$  and friction coefficient  $f_{vm}$ .
- Tail rotor: the moment of inertia  $I_{t1}$  and friction coefficient  $f_{vt}$ .
- Pitch angle: the moment of inertia  $I_\psi$ , friction coefficients  $f_{v\psi}$  and  $f_{c\psi}$ .
- Yaw angle: the moment of inertia  $I_\phi$ , friction coefficients  $f_{v\phi}$  and  $f_{c\phi}$ .

Table 2: Model parameters

parameter	est. value	tuned value	unit
$I_{m1}$	$4.13 \times 10^{-4}$	$1.72 \times 10^{-4}$	kg m <sup>2</sup>
$I_{t1}$	$1.49 \times 10^{-4}$	$3.24 \times 10^{-5}$	kg m <sup>2</sup>
$I_\psi$	0.0651	0.0656	kg m <sup>2</sup>
$I_\phi$	0.0113	0.0113	kg m <sup>2</sup>
$I_c$	0.0537	-	kg m <sup>2</sup>
$f_{v\psi}$	0.006	0.0024	N m rad <sup>-1</sup> s
$f_{c\psi}$	0.001	$5.69 \times 10^{-4}$	N m
$f_{v\phi}$	0.1	0.03	N m rad <sup>-1</sup> s
$f_{c\phi}$	0.02	$3 \times 10^{-4}$	N m
$f_{vm}$	$4.5 \times 10^{-5}$	$3.89 \times 10^{-6}$	N m rad <sup>-1</sup> s
$f_{vt}$	$2.3 \times 10^{-5}$	$3.43 \times 10^{-6}$	N m rad <sup>-1</sup> s
$C_{Tm}^+$	$1.53 \times 10^{-5}$	-	N s <sup>2</sup> rad <sup>-2</sup>
$C_{Tm}^-$	$8.8 \times 10^{-6}$	-	N s <sup>2</sup> rad <sup>-2</sup>
$C_{Tt}^+$	$3.25 \times 10^{-6}$	-	N s <sup>2</sup> rad <sup>-2</sup>
$C_{Tt}^-$	$1.72 \times 10^{-6}$	-	N s <sup>2</sup> rad <sup>-2</sup>
$C_{Rm}^+, C_{Qm}^+$	$4.9 \times 10^{-7}$	-	N m s <sup>2</sup> rad <sup>-2</sup>
$C_{Rm}^-, C_{Qm}^-$	$4.1 \times 10^{-7}$	-	N m s <sup>2</sup> rad <sup>-2</sup>
$C_{Rt}, C_{Qt}$	$9.70 \times 10^{-8}$	-	N m s <sup>2</sup> rad <sup>-2</sup>
$C_c$	0.016	-	N m rad <sup>-1</sup>
$\psi_0$	-0.6663	-0.5093	rad
$\phi_0$	-0.4602	-	rad
$G_c$	-0.1954	-0.275	N m
$G_s$	0.1536	-	N m
$H_c$	-0.0012	-	kg m <sup>2</sup>
$H_s$	0.0012	-	kg m <sup>2</sup>

The final parameters of the mathematical model are summarised in Table 2.

## 4 SIMULATION

The conformity of the mathematical model with the real plant was assessed qualitatively using a set of tests, in which the open-loop responses, of the model and of the real plant, to the same inputs were compared. Note that, in the TRMS setup, the actual yaw and tail rotor angles are measured in the opposite directions from those used in the model [3]. Hence, the relevant signs were changed accordingly. By inspecting the obtained results (Fig. 10 to 13) we can say that the model captures fairly accurately the behaviour of the real system. The obtained mathematical model was used in the synthesis of a non-linear  $H_\infty$  control law [6]. Some closed-loop responses are displayed in Fig. 14 to 15.

## 5 CONCLUSIONS

In this work we have developed a complete dynamic model of the TRMS. The parameters of the model were estimated and tuned using experimental data.

The model was subsequently used to design a controller for the TRMS. Further details about the implementation of the controller will be reported elsewhere. The object of future work will be the design of an anti wind-up scheme to compensate for inputs' saturation.

## Copyright Statement

The authors confirm that they, and/or their company or organization, hold copyright on all of the original material included in this paper. The authors also confirm that they have obtained permission, from the copyright holder of any third party material included in this paper, to publish it as part of their paper. The authors confirm that they give permission, or have obtained permission from the copyright holder of this paper, for the publication and distribution of this paper as part of the ERF2013 proceedings or as individual offprints from the proceedings and for inclusion in a freely accessible web-based repository.

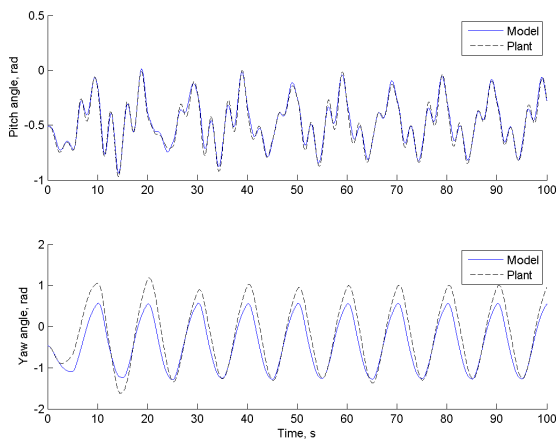


Figure 10: Model vs. plant responses to square input along pitch angle

## References

- [1] Alain J. Brizard. *An introduction to Lagrangian mechanics*. World Scientific, 2008.
- [2] Feedback Instruments. *Twin Rotor MIMO System. Advanced Teaching Manual 1. 33-007-4M5*. Feedback Instruments Ltd., Park Road, Crowborough, East Sussex, TN6 2QR, UK, 01 edition, 09 1998.
- [3] Feedback Instruments. *Twin Rotor MIMO System Control Experiments. 33-949S*. Feedback Instruments Ltd., Park Road, Crowborough, East Sussex, TN6 2QR, UK, 01 edition, 12 2006.

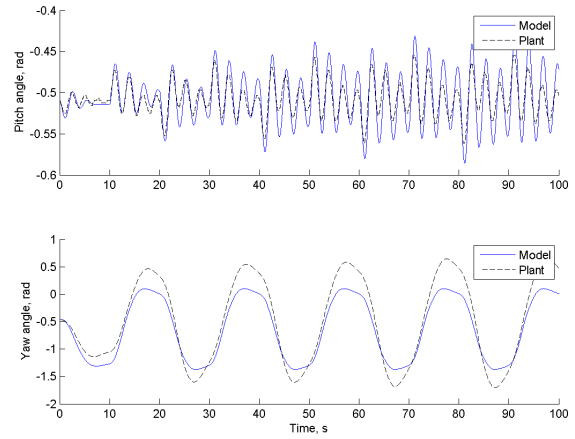


Figure 11: Model vs. plant responses to square input along yaw angle

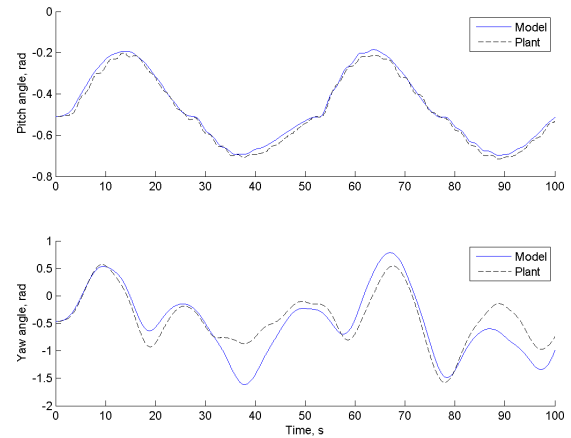


Figure 12: Model vs. plant responses to simultaneous sine inputs along both angles

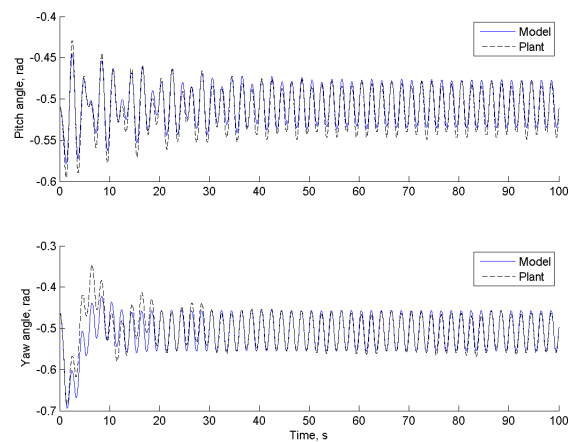


Figure 13: Model vs. plant responses to simultaneous square inputs along both angles

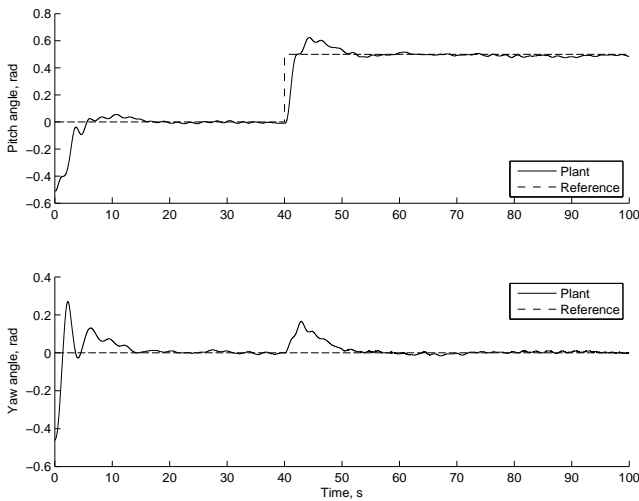


Figure 14: Closed-loop step response along pitch angle

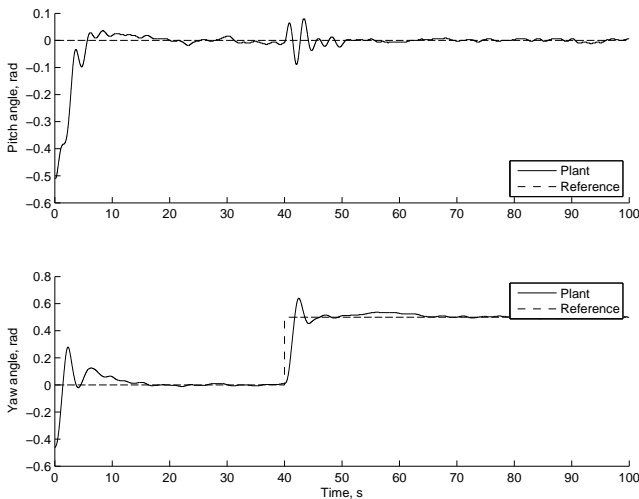


Figure 15: Closed-loop step response along yaw angle

- [8] A Rahideh and M. H. Shaheed. Mathematical dynamic modelling of a twin-rotor multiple input-multiple output system. *Proceedings of the Institution of Mechanical Engineers, Part I: Journal of Systems and Control Engineering*, 221(1):89–101, 2007.
- [9] N. Woodhouse. *Introduction to Analytical Dynamics*. Springer Undergraduate Mathematics Series. Springer, 2009.
- [4] E.L. Houghton and A.E. Brock. *Aerodynamics for Engineering Students*. Edward Arnold, 1982.
- [5] R. Kelly, J. Llamas, and R. Campa. A measurement procedure for viscous and coulomb friction. *Instrumentation and Measurement, IEEE Transactions on*, 49(4):857–861, aug 2000.
- [6] M. Lopez-Martinez, M.G. Ortega, C. Vivas, and F.R. Rubio. Nonlinear control of a laboratory helicopter with variable speed rotors. *Automatica*, 43(4):655 – 661, 2007.
- [7] Philippe Mullhaupt, Balasubrahmanyam Srinivasan, Jean Levine, and Dominique Bonvin. Control of the toycopter using a flat approximation. *IEEE Transactions on Control Systems Technology*, 16(5):882–896, 2008.